ENERGY EFFECTIVENESS AND WORKING CHARACTERISTICS OF DIFFERENT TOWER REACTORS FOR AERATED SLURRY SYSTEMS

Serafim D. VLAEV[a] and Jindřich ZAHRADNÍK[b]

[a] *Institute of Chemical Engineering, Bulgarian Academy of Sciences, Sofia 1113, Bulgaria and*
[b] *Institute of Chemical Process Fundamentals, Czechoslovak Academy of Sciences, 165 02 Prague 6-Suchdol, Czechoslovakia*

Received March 9th, 1987

Decisive hydrodynamic and mass transfer characteristics of different types of tower reactors (rotating disc reactor, single and multistage sieve-tray bubble columns, tower reactor with ejector gas distributor) as well as the energy effectiveness of their performance were compared with the purpose to establish a quantitative basis for the qualified choice of the proper reactor type according to demands of specific reaction processes. Selected design parameters included gas and solid phase holdup, $k_L a_L$, liquid phase residence time distribution, and axial distribution of the solid phase, the experiments were carried out in a wide range of solid phase concentration (0–20 wt. %) and particle sizes (2·3–280 μm). The experimental results proved that due to their favourable suspension characteristics and operation stability the rotating disc reactors can be advantageously used for slow reaction processes with low demands on the intensity of interfacial gas–liquid contact which can be carried out at low gas flow rates. On the other hand the multistage bubble column reactors proved to be superior devices for transport-controlled reaction processes regarding both the achievable rate of interfacial mass transfer and the overall energetic efficiency of phase contacting.

The increasing tendency towards tailoring the multiphase reactors for gas–liquid and gas–liquid–solid(slurry) systems as closely as possible to specific demands of individual chemical and biotechnological processes resulted lately in the appearance of numerous novel types of these reactors developed as alternatives to classical aerated stirred tank and bubble column reactors. Among the requirements to be considered in the reactor design the most frequently encountered are intensification of the interfacial (gas–liquid, liquid–solid) mass transfer and optimization of flow patterns of individual phases from the viewpoint of maximum reaction rate and/or selectivity. Regarding the latter requirement a modified type of the rotating disc reactor was recently constructed and tested[1–3] for gas–liquid–solid (slurry) systems. It was assumed that the reactor construction could ensure good axial and radial distribution of the solid phase at relatively low demands on the energy supply and that the character of liquid flow would be stable and well defined within wide ranges of gas and liquid flow rates and discs rotation speed. While the validity of such assumptions was confirmed for the major part by the results of our studies[1–3] mentioned above,

further, more thorough examination of the rotating disc reactor performance was apparently desirable aimed at the establishing of a sound quantitative basis for the design of such reactors. To approach this goal, our present work was devoted to the determination of decisive hydrodynamic and mass transfer characteristics of rotating disc reactors (gas and solid phase holdup, $k_L a_L$, liquid phase residence time distribution, axial distribution of the solid phase) and to the evaluation of the energy effectiveness of their performance. It was our purpose to compare the values of these design parameters with those obtained for other gas–liquid–solid contacting devices and to define on the basis of such comparison the optimum working region of rotating disc reactors.

EXPERIMENTAL

Schematic chart of the experimental rotating disc reactor is shown in Fig. 1. Glass-wall column 1 0·14 m in diameter was divided into five compartments by horizontal baffles 2 with central openings. Two perforated discs mounted on the centrally located shaft 3 were installed in each compartment, one of them 4 in the middle of the compartment height, the other one 5 in the distance of 5 mm above baffles. For construction reasons, diameters of discs and central openings were slightly different in individual stages, average diameter values equaled to 0·08 and 0·076 m for discs and central openings respectively. Diameter of discs perforations was 1·9 mm, free perforations area equaled to 2%. Overall column height was 0·55 m. The height of compartments 2—5 was constant and equaled to 0·1 m, the upper stage height was designed to allow free bed expansion. Gas was introduced at the column bottom 6, liquid–solid suspension was fed countercurrently to the top of the column 7 and left the reactor *via* the overflow vessel 8.

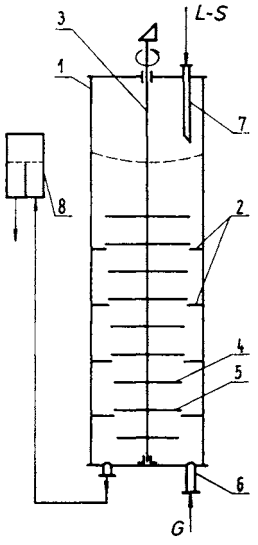

FIG. 1

Schematic chart of the rotating disc reactor. 1 Reactor vessel, 2 horizontal baffles, 3 shaft, 4, 5 perforated discs, 6 gas supply, 7 suspension inlet tube, 8 overflow vessel

Corresponding data from bubble bed tower reactors were obtained in single and multistage bubble columns with perforated gas distributing plates and in the tower reactor with the ejector-type gas distributor. Detailed description of these referential units shown schematically in Fig. 2 can be found in original papers[4-7]. Geometrical characteristics of individual reactors and corresponding gas distributing devices are given in Table I.

Air and tap water were used as gaseous and liquid phase, solid phases included glass beads ($d_p = 24-280$ μm), silicon carbide ($d_p = 10-60$ μm), and zinc oxide ($d_p \approx 2{\cdot}3$ μm). Experiments were performed within the range of solid phase concentrations 0—20 mass %. Measured variables included gas and solid phase holdup, volumetric liquid side mass transfer coefficient ($k_L a_L$), residence time distribution of the liquid (suspension) phase and axial distribution of the solid phase. The power input of the rotating disc reactor was also determined and alternatively, the

TABLE I

Geometrical parameters of experimental bubble-bed reactors

Sieve-tray bubble columns	Tower reactor with ejector distributor
$D_c = 0{\cdot}14$; $0{\cdot}30$ ms^{-1}	$D_c = 0{\cdot}30$ m
$N_c = 1$; 3; 5	$L_d = 0{\cdot}40$ m
$d_o = 0{\cdot}5$; 1·0; 1·6 mm	$\alpha = 1{\cdot}7°$
$\varphi = 0{\cdot}1$; 0·2%	$d_n = 8$ mm

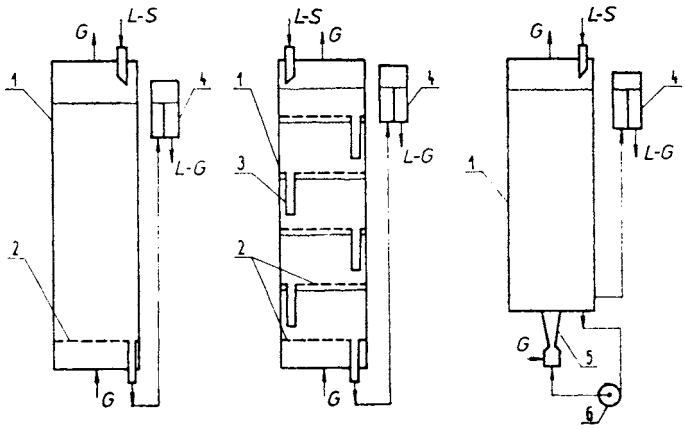

a *b* *c*

FIG. 2

Schematic charts of referential bubble-bed tower reactors. *a* Sieve-tray bubble column reactor; *b* multistage bubble column reactor; *c* tower reactor with ejector gas distributor; 1 reactor vessel, 2 distributing plates, 3 downcomer tubes, 4 overflow vessel, 5 ejector, 6 pump

wetted plate pressure drop and the circulation pump discharge pressure were measured in units with sieve tray and ejector-type gas distributors. The specific rate of energy dissipation related to a unit of liquid (suspension) mass, e_d, was then calculated for individual contactors used and respective values of energy effectiveness parameters, $\Phi = k_L a_L / e_d$, introduced in our former paper[8], were evaluated from experimental data.

Values of gas holdup in the rotating disc reactor and in the single stage bubble column were obtained by the combination of bed expansion and stop flow methods, method of pressure differences[9] was used for gas holdup determination in the multistage bubble column. Local values of solid phase holdup were determined by weighing the solids content of suspension samples taken from specific positions of the bubble bed. Values of $k_L a_L$ were obtained by physical absorption of CO_2 in water using the steady state technique described in details elsewhere[1]. Alternatively, dynamic or steady-state physical methods of $k_L a_L$ measurement were used in single or multistage units respectively, based upon monitoring the oxygen concentration in liquid (suspension) phase. The Clark-type fast response polarographic electrodes were used for dissolved oxygen concentration measurement, details of experimental procedures can be found *e.g.* in papers of Kratochvíl and co-workers[4] (dynamic method) or Deckwer, Burghart and Zoll[10] (steady--state method). Preliminary experiments proved good compatibility of $k_L a_L$ data obtained by the respective methods within the whole range of our experimental conditions. Conductivity method was used for determination of liquid phase residence time distribution. System response to a pulse input signal of the tracer (aqueous solution of KCl) was measured at the column outlet by the conductivity probe and the experimental curves were subsequently transformed to a dimensionless form corresponding to C-curves defined by Levenspiel[11]. Single parameter backflow cell model was chosen for description of axial phase mixing in sectionalized units (rotating disc reactor, multistage buble column reactor) and the backmixing coefficient, f_e, characterizing the interstage liquid backflow was evaluated from the comparison of experimental curves with RTD data calculated from the model equation[3]

$$\frac{V_j}{V_r} \cdot \frac{\mathrm{d}C_j}{\mathrm{d}\Theta} = f_e(C_{j-1} + C_{j+1} - 2C_j) + (C_{j-1} - C_j), \qquad (I)$$

where C is dimensionless tracer concentration, Θ dimensionless time, V_r reactor volume and subscript j refers to an individual stage.

Mixing power input in the rotating disc reactor was determined by the standard compensation method[12]. The pump discharge pressure was measured by a calibrated manometer, values of wetted plate pressure drop were calculated from readings of pressure taps situated below and above distributing plates.

RESULTS AND DISCUSSION

Hydrodynamic and Mass Transfer Characteristics

Relatively high values of gas holdup were observed at low gas flow rates in the rotating disc reactor even compared to other apparatuses recommended for intensive gas–liquid contacting such as multistage sieve-tray column or tower reactor with the ejector gas distributor. As an illustration, gas holdup data obtained at identical experimental conditions (SiC, $d_p = 30\ \mu m$, $c_s = 6$ mass %) in the rotating disc reactor, single and multistage ($N_c = 5$) bubble columns and in the reactor with the

ejector (Venturi tube) gas distributor are plotted in Fig. 3 as a function of superficial gas velocity. Gas holdup in the rotating disc reactor decreased with increasing rotation speed in the range of linear mixing velocities $n\langle d_m\rangle = 0{\cdot}3-1{\cdot}0\ \mathrm{m\,s^{-1}}$ (see *e.g.* data for $n\langle d_m\rangle = 0{\cdot}33$ and $0{\cdot}60\ \mathrm{m\,s^{-1}}$ plotted in Fig. 3). Quite understandably the experimental evidence proved positive effect of bubble column sectionalization on gas holdup in the system and confirmed also good quality of gas–liquid dispersion created in units with ejector gas distributors.

Corresponding data k_La_L *vs* u_G for all types of reactors studied are plotted in Fig. 4. Similarly as gas holdup values even these data confirmed efficient performance of the rotating disc reactor at extremely low gas flow rates ($u_G < 0{\cdot}01$ m/s) *i.e.* at conditions when the application of other types of contactors becomes questionable due to problems with uniform gas distribution (see the dash lines in Fig. 4 corresponding to hypothetical "starting" sections of dependences k_La_L *vs* u_G beyond the operation region of respective contacting devices used). On the contrary to gas holdup data only minor increase of k_La_L with increasing gas flow rate was however observed in the rotating disc reactor and consequently rather low values of k_La_L were achieved in this reactor at superficial gas velocities $u_G \geqq 0{\cdot}01\ \mathrm{m\,s^{-1}}$. Apparently thus, the increase of gas holdup with increasing gas flow rate was in the rotating disc reactor

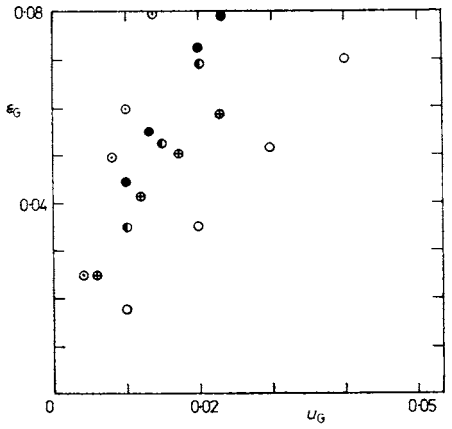

FIG. 3

Gas holdup as a function of superficial gas velocity, u_G ($\mathrm{m\,s^{-1}}$); SiC particles, $d_p = 30\ \mu\mathrm{m}$, $c_s = 6$ wt. % rotating disc reactor: ⊙ $n\langle d_m\rangle = 0{\cdot}33\ \mathrm{m\,s^{-1}}$, ⊕ $n\langle d_m\rangle = 0{\cdot}60\ \mathrm{m\,s^{-1}}$; bubble column reactor ($d_o = 1{\cdot}6$ mm, $\varphi = 0{\cdot}2\%$): ○ single stage, ● five stages, ◐ tower reactor with ejector distributor ($L_d = 0{\cdot}4$ m, $d_n = 8$ mm)

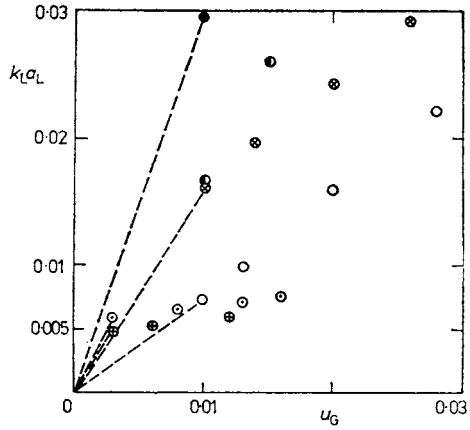

FIG. 4

Volumetric liquid-side mass transfer coefficient, $k_La_L(\mathrm{s^{-1}})$, as a function of superficial gas velocity, $u_G(\mathrm{m\,s^{-1}})$; $d_p = 20\ \mu\mathrm{m}$, $c_s = 5$ wt. %; Rotating disc reactor: ⊙ $n\langle d_m\rangle = 0{\cdot}33\ \mathrm{m\,s^{-1}}$, ⊕ $n\langle d_m\rangle = 0{\cdot}60\ \mathrm{m\,s^{-1}}$; bubble column reactor: ○ $N_c = 1$, ● $N_c = 3$, ⊗ $N_c = 5$; ◐ tower reactor with ejector distributor

not accompanied by the corresponding increase of $k_L a_L$ characterizing the intensity of interfacial (gas–liquid) mass transfer. This is clearly demonstrated by the shape of the dependence $k_L a_L$ on gas holdup plotted for rotating disc reactor in comparison with other reactor types in Fig. 5. Different shapes of dependences $k_L a_L$ *vs* ε_G for bubble column reactors and for the rotating disc reactor respectively suggest that, due to different mode of gas–liquid dispersion formation, the unambiguous relation between gas holdup and specific interfacial area (and consequently also $k_L a_L$) proved experimentally in bubble column reactors with both sieve-tray and ejector gas distributors[8] is not valid in rotating disc reactors and consequently thus higher intensity of gas–liquid mass transfer in these devices cannot be achieved just by the gas holdup increase. Also, the data in Fig. 5 proved that the relation between $k_L a_L$ and gas holdup in the rotating disc reactor was only slightly influenced by the discs rotation speed (linear mixing velocity) *i.e.* that the mixing intensity did not alter significantly the mechanism of gas–liquid mass transfer represented by values of k_L.

As can be seen from the data for the single-stage bubble column reactor plotted in Fig. 5, the dependence $k_L a_L$ *vs* ε_G was not influenced by the solid phase concentration (in the region $c_s = 2{\cdot}5 - 10$ mass %). This is in agreement with the assumption that, except for extremely small particles, the character of mass transfer between gaseous and liquid phase is not altered by the presence of the solid phase and the changes of $k_L a_L$ with c_s are caused solely by variations of the interfacial area due to changes of gas holdup[5].

Energetic Efficiency of Reactor Performance

To estimate the efficiency of gas dispersion and/or to compare the energetic performance of various types of gas–liquid or gas–liquid–solid (slurry) contactors,

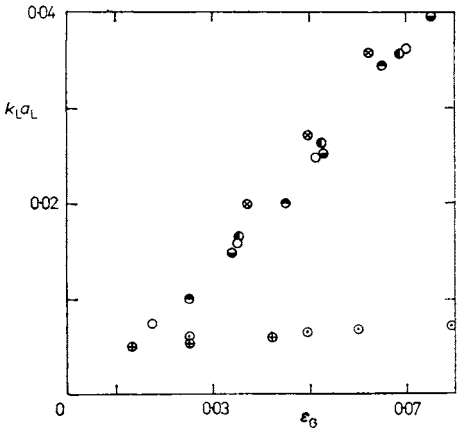

FIG. 5

Relation between $k_L a_L (s^{-1})$ and gas holdup ratio, ε_G. Rotating disc reactor ($c_s =$ = 5 wt. %): ⊙ $n\langle d_m \rangle = 0{\cdot}33$ m s^{-1}, ⊕ $n\langle d_m \rangle = 0{\cdot}60$ m s^{-1}; single-stage bubble column reactor: ◓ $c_s = 2{\cdot}5$ wt. %, ○ $c_s =$ = 5 wt. %, ○ $c_s = 10$ wt. %; ◒ multistage bubble column reactor ($N = 3$), $c_s = 5$ wt. %

the energy effectiveness criterion, Φ, was introduced in our former paper[8], defined as the ratio of $k_L a_L$ and the specific rate of energy dissipation corresponding to gas–liquid dispersion formation ($\Phi = k_L a_L / e_d$). Multiplied by the mass transfer driving force (concentration gradient) this parameter represents the amount of mass transferred between the gaseous and liquid phase *per* a unit of dissipated energy. According to definition, following relations can be written for the rate of energy dissipation (related to a unit of suspension mass) in buble column reactors and in tower reactors with ejector gas distributors[8]:

$$e_{db} = (\Delta P_h + \Delta P_{wp})\, \dot{V}_G / V_{sl} \varrho_{sl} \qquad (2)$$

(sieve-tray bubble columns) and

$$e_{de} = \Delta P_e Q_{sl} / V_{sl} \varrho_{sl} \qquad (3)$$

(ejector-distributor reactor).

In Eqs (2) and (3) ΔP_h denotes hydrostatic pressure of the bed, ΔP_{wp} wetted plate pressure drop, ΔP_e ejector pressure drop, V_{sl} is the total volume of liquid–solid suspension (slurry) in the reactor, and ϱ_{sl} is the slurry density defined by Brinkmann[13] as

$$\varrho_{sl} = \varepsilon_s \varrho_s + (1 - \varepsilon_s)\, \varrho_L \,.$$

Analogically, for the rotating disc reactor

$$e_d = (N + \Delta P_h \dot{V}_G) / V_{sl} \varrho_{sl} \,, \qquad (4)$$

where N is the energy transferred by rotating discs to the suspension *per* a time unit and $\Delta P_h \dot{V}_G$ is the rate of energy dissipation in gaseous phase. In Table II, these two contributions to the overall dissipation rate are compared in dependence on the gas flow rate and linear mixing velocity (stirrer rotation speed). Apparently the contribution of the energy dissipated by the discs was almost negligible at low linear mixing velocities ($n\langle d_m \rangle \leqq 0{\cdot}2\ \mathrm{m\,s^{-1}}$) and it became predominant only at high rotation speeds (see data for $n\langle d_m \rangle = 0{\cdot}8$ and $1{\cdot}1\ \mathrm{m\,s^{-1}}$). Such results obviously prove extremely low energetic demands of rotating disc reactors in the region of low and medium discs rotation speed. It should be stressed that our experimental values of energy amount transferred *per* time unit from rotating discs to the suspension, N, agreed within the whole experimental range of rotation speed fairly well with data obtained from the graph $\mathrm{Ne} = \mathrm{Ne}(\mathrm{Re_r})$ presented by Brauer[14] for liquid phase rotating disc reactors and corrected for the conditions of aerated beds[14]. Values of dimensionless Newton and Reynolds numbers were determined from their definition relations, $\mathrm{Ne} = N / n^3 d_m^5 \varrho_{sl}$, $\mathrm{Re_r} = n d_m^2 / \nu_{sl}$, where the kinematic viscosity of the slurry phase, $\nu_{sl} = \mu_{sl} / \varrho_{sl}$, was calculated using the Roscoe's relation[15] for the dynamic viscosity, $\mu_{sl} = \mu_L (1 - \varepsilon_s)^{-2.5}$.

In Fig. 6, values of parameter Φ are plotted against $k_L a_L$. Experimental data obtained in the rotating disc reactor at different rotation speeds and gas flow rates are compared with average experimental dependences (denoted by solid lines) determined previously[8] in the sieve-tray bubble column reactor (within the range of free plate areas $\varphi = 0{\cdot}2 - 1{\cdot}0\%$) and in the tower reactor with ejector distributor. The dashed sections of these lines denote again extrapolation of the dependences beyond the operational region of respective reactors (*i.e.* below the lowest experimental values of $k_L a_L$ obtained in these reactors). As for the data from the rotating disc reactor, points plotted at higher $k_L a_L$ values (for each rotation speed) correspond to higher gas flow rates (appropriate values u_G corresponding to individual pairs Φ–$k_L a_L$ are given in Table II).

The graph clearly proves high energetic efficiency of the rotating disc reactor at low stirring speeds ($n \leqq 2{\cdot}5\ s^{-1}$) and gas flow rates *i.e.* in the region of low $k_L a_L$

TABLE II

Energy effectiveness of gas–liquid contacting in rotating disc reactor — comparison of contributions to the overall energy dissipation rate

$n\langle d_m \rangle$ m s^{-1}	u_G m s^{-1}	$N/(V_{sl} \cdot \varrho_{sl})$ W kg^{-1}	$\Delta P_h V_G/(V_{sl} \cdot \varrho_{sl})$ W kg^{-1}	e_d W kg^{-1}	$k_L a_L$ s^{-1}	Φ kg J^{-1}
0	0·003	0	0·030	0·030	0·0039	0·130
0·1	0·003	0·002	0·030	0·032	0·0040	0·125
0·2	0·003	0·007	0·030	0·037	0·0056	0·151
0·2	0·007	0·007	0·064	0·071	0·0063	0·089
0·2	0·009	0·007	0·085	0·092	0·0064	0·070
0·2	0·014	0·007	0·136	0·143	0·0065	0·045
0·2	0·016	0·007	0·158	0·165	0·0072	0·044
0·39	0·003	0·038	0·030	0·068	0·0040	0·059
0·39	0·009	0·038	0·086	0·124	0·0050	0·040
0·60	0·003	0·143	0·030	0·173	0·0053	0·031
0·60	0·007	0·143	0·064	0·207	0·0054	0·026
0·60	0·013	0·143	0·131	0·274	0·0057	0·021
0·80	0·003	0·335	0·030	0·365	0·0026	0·007
1·1	0·003	0·800	0·030	0·830	0·0032	0·004

values. With the increasing rotation speed the energy effectiveness of the rotating disc reactor decreased sharply which is quite understandable considering the ambiguous relation between the amount of energy transferred to the bed and $k_L a_L$ values observed (see Table II). Similarly, the decrease of the energy effectiveness with increasing gas flow rate confirmed that the minor increase of $k_L a_L$ with u_G in the rotating disc reactor (see Fig. 4) did not make up for the increase of the energy dissipation rate. Results of our experiments proved further that for the specific reactor configuration used, $n = 2{\cdot}5\ s^{-1}$ can be considered as the optimum discs rotation speed regarding both maximum $k_L a_L$ values and the highest energy effectiveness of the unit.

Considering the data for different reactor types presented in Fig. 6 it can be concluded that, regarding the energetic efficiency of gas–liquid contacting, application of the rotating disc reactor cannot be recommended when demands on the rate of gas–liquid mass transfer correspond to $k_L a_L$ values higher than $0{\cdot}0075\ s^{-1}$. Below this limiting value such a reactor can be however advantageously applied both for its efficient performance and operation stability.

Solids and Liquid Phase Distribution

The average solids content in the rotating disc reactor characterized by values of solid phase holdup, ε_s, was almost independent of the linear mixing velocity (or, for $\langle d_m \rangle$ = const., of the discs rotation speed), these variables however influenced solid phase distribution along the reactor height. In agreement with our former results[2] solids holdup in the upper reactor stage increased with decreasing $n\langle d_m \rangle$ to the detriment of solids concentration in the bottom stage. Apparently such variations of local solids holdup can be ascribed to the increased extent of solids entrainment at lower

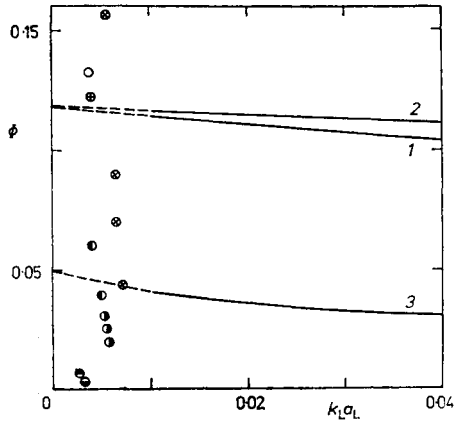

FIG. 6

Relation between energy effectiveness criterion, Φ (kg J^{-1}), and $k_L a_L$ (s^{-1}). Rotating disc reactor: ○ $n\langle d_m \rangle = 0$, ⊕ $n\langle d_m \rangle = 0{\cdot}1\ m\ s^{-1}$, ⊗ $n\langle d_m \rangle = 0{\cdot}2\ m\ s^{-1}$, ◐ $n\langle d_m \rangle = 0{\cdot}33\ m\ s^{-1}$, ◑ $n\langle d_m \rangle = 0{\cdot}6\ m\ .\ s^{-1}$, ◓ $n\langle d_m \rangle = 0{\cdot}8\ m\ s^{-1}$, ◒ $n\langle d_m \rangle = 1{\cdot}1\ m\ s^{-1}$; solid lines: *1* bubble column reactor, $\varphi = 0{\cdot}2\%$, $d_o = 1{\cdot}6$ mm; *2* $\varphi = 1\%$, $d_o = 1{\cdot}6$ mm; *3* tower reactor with ejector distributor ($L_d = 0{\cdot}4$ m, $d_n = 6-10$ mm)

stirring speeds. On the other hand, the increase of solids hold up in lower rector stages with increasing $n\langle d_m\rangle$ can be explained by the suction effect of rotating discs. As an illustration, data of solids holdup ($\bar{\varepsilon}_s$, ε_{sl}, ε_{s5}) obtained for particles diameter 27 μm in the range of linear mixing velocities, $n\langle d_m\rangle = 0{\cdot}3-0{\cdot}9$ m s^{-1}, at $u_G =$ $= 0{\cdot}013$ m s^{-1} are plotted in Fig. 7 against the linear mixing velocity, $n\langle d_m\rangle$. As can be seen from the figure, the average solid phase holdup decreased only slightly from 1·72 to 1·68% within the whole range of $n\langle d_m\rangle$.

Experimental results proved also that good axial and radial distribution of the solid phase can be achieved in the rotating disc reactor just due to stirring effect of the discs (*i.e.* even at zero gas flow rate) and thus at low energy consumption. Comparison of its suspension ability with that of standard single stage bubble column reactor proved the superiority of the rotating disc reactor regarding the energetic efficiency of the solid phase fluidization. As an illustration the average values of solid phase concentration, c_s, determined in the two reactors for different particle sizes were plotted in Fig. 8 against the initial suspension concentration, c_{so}. Apparently, at zero gas flow rate c_s equals to the solid phase holdup, ε_s, in the reactor. As can be seen from the figure, the values of solid phase concentration achieved in the rotating disc reactor at the linear mixing velocity $n\langle d_m\rangle = 0{\cdot}33$ m s^{-1} and zero gas

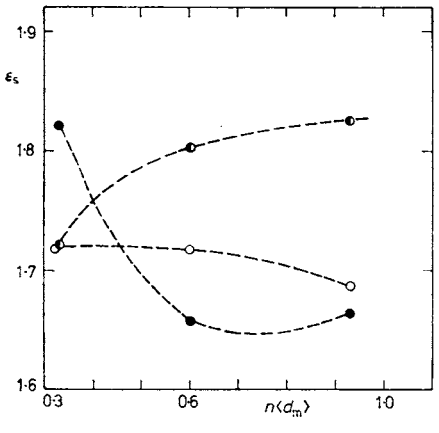

FIG. 7

Solids holdup in rotating disc reactor as a function of linear mixing velocity, $n\langle d_m\rangle$ (m s^{-1}); $d_p = 27$ μm, $u_G = 0{\cdot}013$ m s^{-1}. ○ Average value, ◐ bottom stage, ● upper stage

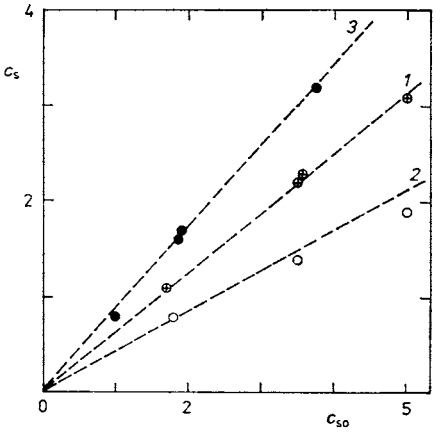

FIG. 8

Suspension ability of rotating disc- and single-stage bubble column reactor (c_s and c_{so} in vol. %). Rotating disc reactor ($n\langle d_m\rangle =$ $= 0{\cdot}33$ m s^{-1}, $u_G = 0$): ⊕ $d_p = 27$ μm, ○ $d_p = 58$ μm, ● $d_p = 10$ μm; bubble column reactor ($u_G = 0{\cdot}018$ m s^{-1}). Dash lines: *1* $d_p = 27$ μm, *2* $d_p = 58$ μm, *3* $d_p = 10$ μm

throughput were in the whole experimental range of c_{so} and d_p almost identical with that determined experimentally in the sieve-tray bubble column reactor at the superficial gas velocity $u_G = 0{\cdot}018\ \mathrm{m\,s^{-1}}$ (dashed lines in Fig. 8). The value of energy consumption rate corresponding to such identical suspension degree was 0·024 W/kg for the rotating disc reactor in comparison with $e_d = 0{\cdot}18$ W/kg for the bubble column reactor. Obviously thus, such result further confirmed that the rotating disc reactors can be used advantageously for operations in slurry systems at low gas flow rates.

A typical *C*-curve characterizing the liquid-phase residence time distribution in the rotating disc reactor is shown in Fig. 9 (curve *1*: $n = 10\ \mathrm{s^{-1}}$, $u_L = 5{\cdot}4 \,.\, 10^{-4}\ \mathrm{m\,s^{-1}}$, $c_s = 10$ mass %, $d_p = 27\ \mu\mathrm{m}$) in comparison with the analogical curve obtained at otherwise identical conditions at zero solid phase concentration (curve *2*) and with theoretical curves calculated for the continuous stirred tank reactor (curve *3*) and for the five-stage cascade of perfectly mixed vessels without liquid backflow between individual stages (curve *4*). The comparison of curves *1* and *2* illustrates well our observation that within the whole experimental range of solid phase concentrations ($c_s \leqq 20$ mass %) and particle dimensions ($d_p = 2{\cdot}3 - 280\ \mu\mathrm{m}$) the presence of the solid phase had only negligible effect on the liquid phase residence time distribution (liquid phase mixing) in all types of reactors studied. Indeed such a conclusion was published previously also by Kato and coworkers[16]. Even visual comparison of the residence time distribution curves proved clearly significantly lower extent of liquid backmixing in the rotating disc rector in comparison with stirred vessel reactors or single stage bubble columns in which complete liquid mixing can be also assumed up to the height to diameter ratio equal to five[17,18]. The qualitative analysis of the shape of RTD curves for the rotating disc reactor and/or their comparison with theoretical curves for the CSTR and five-stage cascade (see Fig. 9) suggested that the axial liquid phase mixing in the rotating disc reactor could be suitably represented by the backflow cell model for the cells number equal to the number of the real reactor compartments. Such a model can be described by the system of equations (*1*)

$$\frac{V_j}{V_r} \cdot \frac{\mathrm{d}C_j}{\mathrm{d}\Theta} = f_e(C_{j-1} + C_{j+1} - 2C_j) + (C_{j-1} - C_j) \quad (j = 1, \ldots 5), \qquad (1)$$

where the backflow coefficient f_e has been the function of the discs geometry and rotation speed and flow rates of both phases, $f_e = f_e(n\langle d_m\rangle, u_G, u_L)$. In Fig. 10 f_e data obtained from comparison of experimental *C*-curves with RTD curves calculated from Eq. (*1*) were plotted as a function of the linear mixing velocity, $n\langle d_m\rangle$ (for zero gas flow rate). The graph clearly proves linear dependence of the backflow coefficient on $n\langle d_m\rangle$ (and consequently on the discs rotation speed), this effect was however strongly reduced by the increasing liquid flow rate already at low absolute flow rate

values. As can be seen from Fig. 10, the functional relation $f_e = f_e(n\langle d_m\rangle, u_L)$ was well described by the equation

$$f_e = 1{\cdot}39 \,.\, 10^{-3} \frac{n\langle d_m\rangle}{u_L} + 0{\cdot}552 \qquad (5)$$

presented by Elenkov and Vlaev[2] for the condition of zero gas flow rate. The additional effect of gas flow rate on the backflow coefficient is apparent from Fig. 11. Values f_e increased with increasing gas flow rate, again however this effect was minimized at higher liquid flow rates (despite their low absolute values). In Fig. 11, dependences f_e *vs* u_G determined in the rotating disc reactor at two different liquid flow rates ($u_L = 6 \,.\, 10^{-5}$ and $2{\cdot}4 \,.\, 10^{-4}$ m s^{-1}) are compared with data obtained in the sectionalized bubble column reactor ($N_c = 3$ and 5) within the wide region of liquid flow rates, $u_L = 2{\cdot}5 \,.\, 10^{-4}$–$0{\cdot}01$ m s^{-1} (sieve tray parameters: $\varphi = 0{\cdot}2$ and 4%, $d_o = 1{\cdot}6$ mm). The comparison clearly proves the superiority of the multistage bubble column reactors regarding the demands on the minimum backflow extent and close approximation of the liquid phase plug flow. As can be seen from

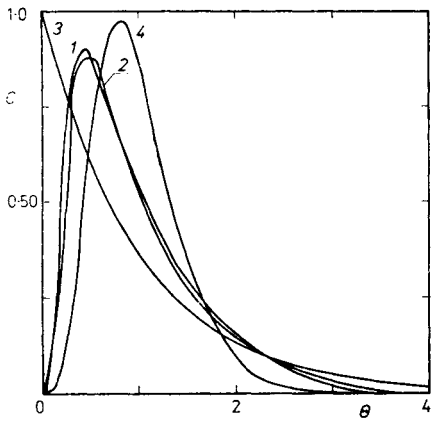

FIG. 9

Residence time distribution curves of liquid and slurry phase in rotating disc reactor — comparison with curves for ideal-flow models. Rotating disc reactor ($n\langle d_m\rangle = 0{\cdot}8$ m s^{-1}, $u_L = 5{\cdot}4 \,.\, 10^{-4}$ m s^{-1}): *1* $c_s = 10$ wt. %, *2* $c_s = 0$; calculated curves: *3* continuous stirred tank reactor, *4* series of five perfectly mixed vessels without liquid backflow between stages

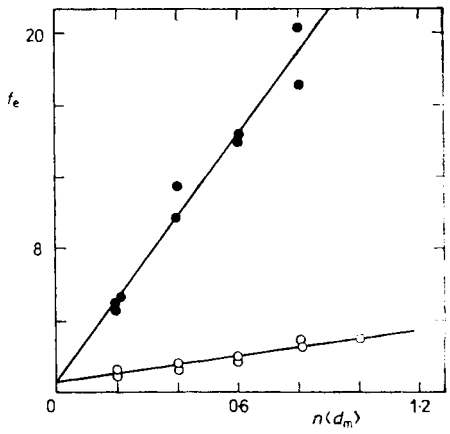

FIG. 10

Coefficient of interstage liquid backflow, f_e, as a function of linear mixing velocity, $n\langle d_m\rangle$ (m s^{-1}). ● $u_L = 5{\cdot}9 \,.\, 10^{-5}$ m s^{-1}, ○ $u_L = 5{\cdot}4 \,.\, 10^{-4}$ m s^{-1}; solid lines: data calculated from Eq. (*5*)

the data plotted in Fig. 11, the interstage backflow coefficient can be significantly reduced in these reactors by the proper design of distributing plates.

Apparently, data plotted in Fig. 11 witness also different backflow mechanisms observed in the two reactor types. Whereas the liquid backflow in the multistage bubble column reator has been caused solely by the upward bubble motion, the liquid macrocirculation induced by the system of rotating discs contributes significantly to the liquid backmixing in reactors of this type. As a result, the backflow coefficient in the rotating disc reactor had even at zero gas flow rate certain finite value (see Fig. 11) corresponding to respective values of discs rotation speed and liquid flow rate (see Eq. (5)).

TABLE III

Comparison of liquid backmixing in rotating disc reactor (RDR) and in multistage bubble column (BCR). $u_L = 2{\cdot}4 \cdot 10^{-4}$ ms^{-1}, $N_c = 5$; RDR: $n = 2{\cdot}5$ s^{-1}, $n\langle d_m\rangle = 0{\cdot}2$ ms^{-1}; BCR 1: $\varphi = 0{\cdot}2\%$, $d_0 = 1{\cdot}6$ mm; BCR 2: $\varphi = 4\%$, $d_0 = 1{\cdot}6$ mm

u_G, ms^{-1}	f_e	Pe	u_G, ms^{-1}	f_e	Pe	u_G, ms^{-1}	f_e	Pe
RDR			BCR 1			BCR 2		
0	1·2	2·94	0·010	0·07	8·8	0·008	0·7	4·2
0·004	1·5	2·50	0·025	0·20	7·1	0·030	2·0	2·0
0·009	1·8	2·17	0·033	0·43	5·4	0·042	3·0	1·4
0·013	2·0	2·00	0·050	1·2	2·9	—	—	—

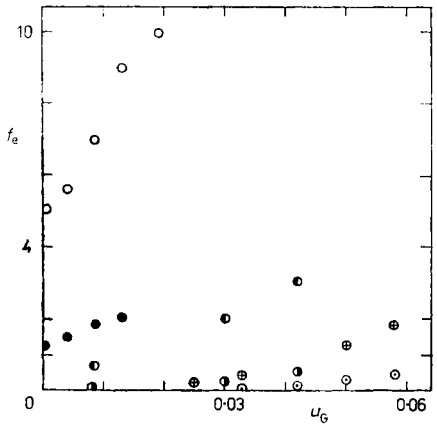

FIG. 11

Dependence of the coefficient of interstage liquid backflow, f_e, on superficial gas velocity, u_G (m s^{-1}) — comparison of data for rotating disc reactor and multistage bubble column with equal number of stages ($N_c = 5$). Rotating disc reactor, $n\langle d_m\rangle = 0{\cdot}2$ m s^{-1}: ○ $u_L = 6 \cdot 10^{-5}$ m s^{-1}, ● $u_L = 2{\cdot}4 \cdot 10^{-4}$ m s^{-1}. Multistage bubble column, $\varphi = 0{\cdot}2\%$, $d_0 = 1{\cdot}6$ mm: ⊕ $u_L = 2{\cdot}5 \cdot 10^{-4}$ m s^{-1}, ⊙ $u_L = 0{\cdot}01$ m s^{-1}; $\varphi = 4\%$, $d_0 = 1{\cdot}6$ mm: ◐ $u_L = 2{\cdot}5 \cdot 10^{-4}$ m s^{-1}, ◑ $u_L = 7{\cdot}5 \cdot 10^{-3}$ m s^{-1}

To establish a general basis for quantitative comparison of liquid flow patterns in sectionalized rotating disc and bubble column reactors, independently of the number of reactor sections, it is suitable to express the extent of liquid backmixing in terms of axial dispersion model *i.e.* to characterize it (without any regard to internal reactor arrangement) by a single parameter – axial dispersion coefficient, D, or alternatively by the dimensionless Peclet number, $\mathrm{Pe} = u_L L/D$. Equation

$$f_e/N_c + 1/2 \,.\, N_c = 1/\mathrm{Pe} \qquad (6)$$

derived by Mecklenburg and Hartland[19] as a representation of the relationship between differential and stagewise RTD models, was therefore used to calculate appropriate values of Peclet number for respective reactor-stage numbers, N_c, and experimental values of backflow coefficient, f_e, determined in both types of reactors at different gas and liquid flow rates.

Comparison of Pe values for rotating disc reactor and sieve-tray bubble column reactor with equal number of stages ($N_c = 5$) is shown in Table III. Data for rotating disc reactor correspond to experiments performed at optimum linear mixing velocity, $n\langle d_m \rangle = 0{\cdot}2 \text{ m s}^{-1}$ (*i.e.* at stirring speed $n = 2{\cdot}5 \text{ s}^{-1}$), liquid flow rate was constant in both reactors, $u_L = 2{\cdot}4 \,.\, 10^{-4} \text{ m s}^{-1}$. Values of Peclet number listed in Table III further confirm that significantly lower extent of liquid backmixing can be achieved in sectionalized bubble columns than in rotating disc reactors at comparable gas and liquid flow rates. Regarding the criteria presented by Levenspiel[11] for estimation of backmixing extent it can be concluded that flow patterns in both types of units are for $N_c = 5$ relatively far from good plug flow approximation ($\mathrm{Pe} \geqq 500$). The rotating disc reactor exhibited within the whole range of experimental conditions (*i.e.* even at zero gas flow rate) large dispersion of liquid ($\mathrm{Pe} \leqq 5$) while liquid flow patterns in five stage bubble column reactor corresponded at low and medium gas flow rates ($u_G \leqq 0{\cdot}03 \text{ m s}^{-1}$) to intermediate backmixing ($5 < \mathrm{Pe} < 500$). Comparison of data determined in bubble column reactor for two geometries of distributing plates ($\varphi = 0{\cdot}2$ and 4%) proved further that the extent of liquid backflow between stages can be significantly reduced by proper design of distributing plates *i.e.* by the use of plates fulfilling the conditions of stable uniform gas distribution[4]. As can be seen in Table III, Pe values corresponding to such a plate ($\varphi = 0{\cdot}2\%$, $d_o = 1{\cdot}6$ mm) approached at low gas flow rates reasonably well theoretical value $\mathrm{Pe} = 10$ calculated for cascade of five perfectly mixed stages without interstage backflow.

SYMBOLS

a_L	specific interfacial area related to a unit of liquid volume
C	dimensionless tracer concentration
c_s	solid phase concentration

D	axial dispersion coefficient
D_c	column diameter
d_m	disc diameter
$\langle d \rangle_m$	average diameter of discs in rotating disc reactor
d_n	ejector-nozzle diameter
d_o	plate hole diameter
d_p	particle diameter
e_d	specific rate of energy dissipation
f_e	coefficient of interstage backflow
k_L	liquid-side mass transfer coefficient
L	reactor length
L_d	length of ejector diffuser
N	energy transferred by rotating discs to liquid
n	disc rotation speed
N_c	total number of cascade stages
$\mathrm{Ne} = N/(nd_m\varrho_{sl})$	dimensionless Newton number
$\mathrm{Pe} = u \,.\, L/D$	dimensionless Peclet number
ΔP_e	ejector pressure drop
ΔP_h	hydrostatic pressure of bubble bed
ΔP_{wp}	wetted-plate pressure drop
$\mathrm{Re}_r = nd_m^2/\nu_{sl}$	dimensionless Reynolds number of slurry phase
u	superficial velocity
V_r	reactor volume
V_{sl}	total volume of slurry phase in the reactor
$\dot{V}$	volumetric flow rate
α	angle of diffuser walls inclination
ε	holdup ratio
Θ	dimensionless time
μ	dynamic viscosity
ν	kinematic viscosity
ϱ	density
σ^2	variance
$\Phi = k_L a_L/e_d$	energy effectiveness parameter
φ	free plate area

Subscripts

G	gaseous phase
j	stage number
L	liquid phase
s	solid phase
sl	slurry

REFERENCES

1. Vlaev S. D.: *Thesis*. Bulgarian Academy of Sciences, Sofia 1981.
2. Elenkov D., Vlaev S. D.: Commun. Dept. Chem. Bulg. Acad. Sci. *15* (2), 196 (1982).
3. Elenkov D., Vlaev S. D. in: *Mass Transfer with Chemical Reaction in Multiphase Systems* (E. Alper, Ed.), Vol. II, pp. 257–266. Martinus Nijhoff Publ., The Hague 1983.

4. Zahradník J., Kaštánek F., Kratochvíl J.: Collect. Czech. Chem. Commun. *47*, 262 (1982).
5. Kratochvíl J., Winkler K., Zahradník J.: Collect. Czech. Chem. Commun. *50*, 48 (1985).
6. Drápal L.: *Thesis*. Institute of Chemical Process Fundamentals, Prague 1987.
7. Zahradník J., Kaštánek F., Kratochvíl J., Rylek M.: Collect. Czech. Chem. Commun. *47*, 1939 (1982).
8. Zahradník J., Kratochvíl J., Kaštánek F., Rylek M.: Chem. Eng. Commun. *15* (1–4), 27 (1982).
9. Zahradník J., Kaštánek F., Rylek M.: Collect. Czech. Chem. Commun. *39*, 1402 (1974).
10. Deckwer W.-D., Burckhart R., Zoll G.: Chem. Eng. Sci. *29*, 2177 (1974).
11. Levenspiel O.: *Chemical Reaction Engineering*. Wiley, New York 1962.
12. Strek F.: *Míchání a míchací zařízení*, p. 247. SNTL – Nakladatelství technické literatury, Prague 1977.
13. Brinkman H. J.: J. Chem. Phys. *20*, 571 (1952).
14. Brauer H.: Ger. Chem. Eng. *3*, 66 (1980).
15. Roscoe R.: Brit. Appl. Phys. *3*, 267 (1952).
16. Kato Y., Nishiwaki A., Fukuda T., Tanaka S.: J. Chem. Eng. Jpn. *5*, 112 (1972).
17. Zahradník J., Kaštánek F.: Collect. Czech. Chem. Commun. *39*, 1419 (1974).
18. Seher A., Schumacher V.: Ger. Chem. Eng. *2*, 117 (1979).
19. Mecklenburg J. C., Hartland S.: *The Theory of Backmixing*, p. 21. Wiley, London 1975.